# Mechanical energy-induced $CO_2$ conversion using liquid metals

**Junma Tang**
University of New South Wales (UNSW)
**Jianbo Tang**
University of New South Wales (UNSW)
**Mohannad Mayyas**
University of New South Wales (UNSW)
**Mohammad B. Ghasemian**
University of New South Wales (UNSW)
**Jing Sun**
University of New South Wales (UNSW)
**Md Arifur Rahim**
University of New South Wales (UNSW)
**Jiong Yang**
University of New South Wales (UNSW)
**Jialuo Han**
University of New South Wales (UNSW)
**Douglas Lawes**
University of New South Wales (UNSW)
**Rouhollah Jalili**
UNSW Sydney https://orcid.org/0000-0003-3851-0818
**Torben Daeneke**
Royal Melbourne Institute of Technology (RMIT)
**Maricruz Saborio**
University of New South Wales (UNSW)
**Zhenbang Cao**
University of New South Wales (UNSW)
**Francois-Marie Allioux**
University of New South Wales (UNSW)
**Anthony O'Mullane**
Queensland University of Technology https://orcid.org/0000-0001-9294-5180
**Richard Kaner**
kaner@chem.ucla.edu https://orcid.org/0000-0003-0345-4924

**Dorna Esrafilzadeh**
University of New South Wales (UNSW)
**Michael Dickey**
North Carolina State University https://orcid.org/0000-0003-1251-1871
**Kourosh Kalantar-Zadeh** ( k.kalantar-zadeh@unsw.edu.au )
University of New South Wales https://orcid.org/0000-0001-6109-132X

**Article**

**Keywords:** Green Carbon Capture, Carbon Conversion Technology, Gallium Liquid Metal, Instantaneous Exfoliation, Nano Dimensional Triboelectrochemical Reactions,

**Posted Date:** December 11th, 2020

**DOI:** https://doi.org/10.21203/rs.3.rs-112257/v1

# Abstract

We report a green carbon capture and conversion technology offering scalability and economic viability for mitigating $CO_2$ emissions. The technology uses suspensions of gallium liquid metal to reduce $CO_2$ into carbonaceous solid products and $O_2$ at near room temperature. The nonpolar nature of the liquid gallium interface allows the solid products to instantaneously exfoliate, hence keeping active sites accessible. The solid co-contributor of silver-gallium rods ensures a cyclic sustainable process. The overall process relies on mechanical energy as the input, which drives nano dimensional triboelectrochemical reactions. By altering the secondary solvent and changing the reactor height, the dissolution and conversion efficiency can be tuned. The optimum reactor height is only 27 cm, when gallium/silver fluoride mix at 7:1 mass ratio is employed as the reaction material. At $CO_2$ input of ~8 sccm, 92% efficiency was obtained at the record low input energy of 228.5 kW•h for the capture and conversion of a tonne of $CO_2$. The potential impact of this green technology is remarkable, likely benefiting a variety of industries and offering an economical solution for $CO_2$ capture and conversion.


# Main Text

Innovative technologies are urgently demanded for capturing and converting $CO_2$ into value-added species, at low input energy, to mitigate the negative effects of this greenhouse gas and support a sustainable carbon cycle[1, 2]. Activating $CO_2$ into $CO_2^{\bullet-}$ radicals or other intermediates is a crucial step for $CO_2$ conversion, while the inertness of $CO_2$ molecules imposes a significant challenge[3]. To this end, external energy is required, and catalytic systems are commonly engaged to lower the energy barrier for $CO_2$ converting. The choices of both the applied energy and functional materials, and how they are pooled together for $CO_2$ conversion govern the efficiency balances. To date, light and electricity have been extensively used as the triggering energies together with many well-known catalytic systems[4-8]. However, in general, the existing electro- or photo- empowered $CO_2$ reduction systems suffer from sluggish reaction rates and high energy consumption. Additionally, there has also been no magical definitive catalyst, that could synergistically operate with these energy types to carry out the conversion at low costs and high efficiencies.

Mechanical energy is easy to generate and often a waste source of energy. Except for organic synthesis and polymerisation[9, 10], mechanical energy has received little attention in catalytic systems and has not yet been utilised for $CO_2$ reduction. In conductive particles suspensions, the introduction of mechanical stimuli can both increase the temperature[11] and generate triboelectrification, as a result of the frictional contact and modulation of gaseous content solubility, respectively[12-14].

Solid metallic catalysts have exhibited excellent performance for electrocatalytic or photocatalytic $CO_2$ reduction[15-17]. However, the active sites of solid metallic catalysts can deteriorate under intense mechanical stimuli and/or can be deactivated when carbonaceous materials adhere onto the catalytic

sites during $CO_2$ reduction. In principle, the use of liquid metals, and specific solid structures, can solve these problems. Gallium (Ga)-based liquid metals have shown intriguing properties for catalysis, including tunability by the incorporation of other elements, and remarkable resistance to coking[18-21] and also excellent mechanical tolerance. Additionally, it is known that Ga (0) can be oxidized to Ga (I) in the presence of organic materials[22]. In this work, we explore whether the same effect can also apply to $CO_2$ and whether we can find a process to reduce Ga(I) back to Ga (0) in a closed cycle stimulated by mechanical agitation. We envision that by employing liquid metal mixes of Ga and a compound of Ag, a closed cyclic catalytic system can be developed. This system can then covert $CO_2$ into value-added species in the reversible Ga-$Ga^+$ cycle, which will be fully explored.

## Assessment of $CO_2$ conversion for various scenarios

We exploited a suspension of Ga and Ag (I) salt mixes as the precursors of the co-catalysts and ultrasound was initially employed to stimulate the $CO_2$ reduction. Dimethylformamide (DMF), with good stability during mechanical agitation and high $CO_2$ solubility of 0.14 M at 40 °C (to assure the liquid state of Ga), was chosen as the solvent[23]. We observed that during the reaction, the $CO_2$ molecules near the interface of the suspended particles were reduced to form carbonaceous sheets in a process that will be detailed later.

The best outcomes were obtained when Ga and AgF were mixed in a DMF solution which also contained 0.10 M HCl to remove the native oxide on the surface of Ga. Ga and AgF were sonicated together (Fig. 1a - using a probe sonicator for 30 min) to generate sub-micron Ga droplets of 230 nm median diameters and $Ag_{0.72}Ga_{0.28}$ rods of micron/sub-micron lengths and median diameters of 160 nm (Fig. 1b and Supplementary Fig. 1). The characterisation outcomes revealing the elemental composition will be presented in a later section.

In the reactor, $CO_2$ was bubbled into and dissolved in DMF through a diffuser (Fig. 1c). The dissolved $CO_2$ is reduced to solid carbonaceous materials at the interface of the Ga droplets. The mechanically enforced $CO_2$ conversion can be scaled up using a variety of mechanical sources that produce frictional contact. To examine this prospect, $CO_2$ conversion by an overhead mixer was also performed and validated (Fig. 1d).

Due to the ultra-smooth nature of the liquid metal droplets, the produced carbonaceous materials on the surface are in the form of sheets[18, 24]. These low dimensional sheets, on the non-polarized liquid metal surface, are exfoliated during mechanical stimulation (Fig. 1e)[18, 24]. Most importantly, the carbon sheets migrate to the top of the reactor and can be isolated due to the density difference with reference to that of metallic components (Fig. 1c,d).

The qualitative and quantitative analyses of the production of carbon, when the Ga/AgF (7.0 to 1.0 mass ratio) suspension in DMF is utilised in a 20 mL reactor, are presented in Fig. 1f and Supplementary Fig. 2. The 7.0 to 1.0 mass ratio and the reaction temperature were chosen according to previously optimised data for C-C bond formation reactions[22]. Additionally, the performance of the system formed by direct alloying of Ga with silver (50 to 1.0 or 20 to 1.0 mass ratio of Ga/Ag, Supplementary Fig. 3e,f) and different silver salts (Fig. 1g-k), including AgCl, AgBr, AgI, AgOTf, $AgNO_3$ (also 7.0 to 1.0 mass ratio) were compared. The homogeneous mixture (20 µL) was drop-casted onto a glass substrate and dried for Raman analysis, with the whole drop-cast region included during the Raman spectroscopy measurement (Supplementary Fig. 3a-d). The changes in the intensity of the carbon D and G bands at 1350 and 1600 $cm^{-1}$, respectively, were employed to obtain the overall picture. Thermal gravimetric analyses (TGA) and gas chromatography (GC) were also conducted for comparative quantitative assessment of the solid carbon and gaseous products (Supplementary Table 1).

For the Ga/AgF system that exhibited the best performance, the production of carbon was observed in < 1 hour of reaction (Fig. 1f) and increased continuously over time according to TGA. The TGA showed that 4.95 mg of carbonaceous materials were produced per hour in a 20 mL reactor at a $CO_2$ flow rate of ~10 sccm (Supplementary Fig. 2). In comparison, the AgCl, AgBr, AgI, and AgOTf mixes also presented $CO_2$ conversion capability, but they were not as efficient as the AgF system (Fig. 1g-j, for brevity only Raman spectra are shown and not TGA). With no emerging D and G bands after 5 hours of reaction (Fig. 1k and Supplementary Fig. 3e,f), Ga/$AgNO_3$ and Ga-Ag alloys were found to be ineffective for $CO_2$ reduction. The reason for these different conversion activities will be discussed later.

To verify that the $CO_2$ reduction relies on the synergism of Ga and AgF, experiments were conducted by employing Ga and AgF separately (Supplementary Fig. 3g,h), both of which resulted in undetectable carbon production. We note that our attempts with other types of salts (e.g. KCl and NaCl) (Supplementary Fig. 3i,j) and magnetic stirring (less powerful in comparison to ultrasonication and overhead stirring) (Supplementary Fig. 3k), showed no carbon formation, indicating the crucial role of the chosen silver salt (AgF) and a threshold for mechanical energy input into the reaction process. Controlled $N_2$ bubbling also did not show any formation of carbonaceous products (Supplementary Fig. 3l).

We explored the minimum co-catalyst mass required in the system to maintain the efficiency of $CO_2$ conversion. Diluting the catalyst by 10 times offered nearly the same conversion efficiency, still achieving an equivalent production of 4.75 mg of carbonaceous materials per hour at ~10 sccm $CO_2$ bubbling rate (Fig. 1l and Supplementary Fig. 2), whereas the output was dramatically reduced for dilutions of 50 or 100 times (Supplementary Fig. 3m,n. TGA profiles are not shown for brevity).

The amount of $CO_2$ dissolved in solution also significantly influenced the efficiency of $CO_2$ conversion. Ethanolamine (ETA) is a suitable choice for increasing this amount since $CO_2$ solubility is 5.6 M in pure ETA[25] in comparison to 0.14 M in DMF at 40 °C. With the addition of 10 vol% ETA in DMF (referred to as DMF+ETA hereafter), $CO_2$ was continuously reduced with a higher efficiency, producing 7.95 mg of

carbonaceous materials per hour in the same reactor at ~10 sccm $CO_2$ bubbling rate (Fig. 1m and Supplementary Fig. 2). Interestingly, 22.2 $cm^3$ CO was also produced in one hour (Supplementary Fig. 4). In contrast, when DMSO or $H_2O$ were used, the efficiency was very low and carbon products could not be quantified by TGA, owing to their limited $CO_2$ solubility (Supplementary Fig. 3o,p).

## Carbonaceous materials characterisation

Carbonaceous materials produced from $CO_2$ were isolated for further characterisation. Scanning electron microscopy (SEM) and energy-dispersive X-ray spectroscopy (EDS) analysis (Fig. 2a and Supplementary Fig. 5a) of the isolated carbonaceous materials reveal that the solid product consists of carbon and oxygen before any secondary washing, with trace quantities of the metallic species that can be easily removed. Fourier transform infrared (FTIR) spectroscopy (Supplementary Fig. 5b,c) further confirms that the carbonaceous materials are primarily comprised of C=C and C-O bonds[18]. Based on X-ray photoelectron spectroscopy (XPS) analysis, the C1s region of the carbonaceous materials shows characteristic peaks of $sp^2$ carbon and C-O bonding, at 284.2 and 286.1 eV, respectively (Supplementary Fig. 5d)[26]. The presence of C-O bonds is validated from the O1s XPS region of the sample (Supplementary Fig. 5e). Transmission electron microscopy (TEM) and selected area electron diffraction (SAED) images demonstrate that part of the carbonaceous material is akin to that of slightly crystalline graphene oxide (Fig. 2b), and a certain proportion of the product exists in the amorphous state (Supplementary Fig. 5f).

## Efficiency and energy requirement for $CO_2$ conversion

The $CO_2$ conversion efficiencies under different configurations were determined using TGA and GC measurements as summarised in Supplementary Table 1 (see Supplementary Information). The conversion efficiency is defined as (captured and reduced $CO_2$/total input $CO_2$)´100%, which are all obtained from the optimum mix of Ga/AgF (to be explained further in the next section).

In the small-volume reactor of 20 mL and height of 4.5 cm, which was used as the characterisation unit in the previous sections, the conversion efficiencies are 1.5% and 6.2%, for DMF and DMF+ETA cases, respectively (Fig. 2c). To demonstrate the scalability, we increased the dimensions of the reactor (Fig. 2d). When the height of the reactor was increased to 40 cm for only DMF solvent (volume of 500 mL), 27% of the input $CO_2$ at the flow rate of ~8.6 sccm could be continuously captured and converted (Fig. 2c). Thus, when the total height of the reactor would be 148 cm, the $CO_2$ conversion could reach the full capacity.

The height of the reactor for near-full conversion could be significantly decreased when DMF+ETA was used as the solvent as this combination could significantly increase the $CO_2$ solubility. The conversion

efficiency reached the unprecedented value of 92% (at the flow of ~8.0 sccm $CO_2$) in this case for a reactor as small as 27 cm in height and 330 mL in volume (Fig. 2c and see Supplementary Fig. 6 for the photo of the set-up). The amount of produced $O_2$ and carbonaceous materials (highly oxidised carbon), under different conditions, are presented in Supplementary Fig. 7 and Supplementary Table 1.

According to these measurements, the total energies required for converting 1.0 tonne of $CO_2$, for DMF and DMF+ETA cases, are obtained as 699.5 kW•h and 228.5 kW•h, respectively (Supplementary Information). An overall estimation based on the current price of electricity suggests that the operational cost of $CO_2$ capture and conversion using DMF+ETA is lower than any other state-of-the-art technologies[27-31].

## Analysis of the suspensions

To elucidate how the functional materials are formed during the probe sonication stage, the reactions between Ga and silver salts were investigated by characterising the sonication products. Sonicating Ga with AgF (as an exemplar) forms an intermetallic phase $Ag_{0.72}Ga_{0.28}$ (Fig. 3a) and $GaF_3$. The existence of metallic Ag (as $Ag_{0.72}Ga_{0.28}$) is confirmed by the Ag3d XPS peaks at 367.8 and 373.8 eV (Fig. 3b)[32]. The metallic fluorides can be verified by the F1s XPS peak at 684.3 eV (Fig. 3c)[33].

The compositions and morphologies of the materials were investigated and correlated with the $CO_2$ reduction performance. As illustrated in Fig. 3a, XRD patterns of Ga mixed with silver salts, which lead to $CO_2$ conversion (i.e., AgF, AgCl, AgBr, AgI and AgOTf), show the presence of $Ag_{0.72}Ga_{0.28}$ crystalline peaks. The control experiments show that $Ag_2Ga$ particles (generated from the sonication of Ga-Ag alloy, Supplementary Fig. 8) and Ag particle inclusions (using Ga/$AgNO_3$ as the precursors, Fig. 3a,d) are inactive materials for $CO_2$ conversion. These results suggest that the formation of $Ag_{0.72}Ga_{0.28}$ is a prerequisite for $CO_2$ reduction. Interestingly, the $Ag_{0.72}Ga_{0.28}$ crystals, generated from different silver salts, show distinct morphologies (Fig. 3e-i and Supplementary Fig. 9) of particles (Fig. 3e-g) or rods (Fig. 3i for AgF) or a combination of both (Fig. 3h for AgCl) together with the Ga spheres. The presence of only rod-shaped morphology (Fig. 3i for AgF) is found to associate with an enhanced $CO_2$ catalytic capability. The Ga/AgF system, which generated the highest efficiency for $CO_2$ conversion, showed the rod-shaped $Ag_{0.72}Ga_{0.28}$, while $Ag_{0.72}Ga_{0.28}$ with non-rod morphology from other silver salts (or limited rod morphology for AgCl) exhibited limited catalytic abilities. The high-resolution TEM images, SAED pattern (Fig. 3j,k) and the TEM-based EDS mapping (Fig. 3l-n) further confirm the existence of the $Ag_{0.72}Ga_{0.28}$ rods and their growth direction along the [201] plane (Fig. 3k). As shown in Fig. 3o-q, the native oxide layer on the surface of the Ga droplets can be observed when dried for analysis. Furthermore, there were no obvious changes to the $Ag_{0.72}Ga_{0.28}$ structures after 5 hours of reaction according to both XRD (Supplementary Fig. 9x) and SEM (Supplementary Fig. 10), indicating that the $Ag_{0.72}Ga_{0.28}$ rods were resilient towards mechanical agitation.

The concentration of gallium and silver ions in solution during the reaction was measured by inductively coupled plasma mass spectrometry (ICP-MS) (Supplementary Fig. 11). The ion concentrations fluctuated without showing any increasing or decreasing trend, indicating that the catalysts are not consumed, and that the system is stoichiometrically stable.

## Reaction mechanism

Based on the configuration of the catalytic process, we can consider a scenario in which the contact of the Ga/DMF interface is altered by the interfacial formation of $CO_2$ bubbles. $CO_2$ bubbles are formed as the Ga/DMF interface becomes warmer due to localised friction[11]. As such, the interfacial solubility of $CO_2$ in DMF decreases. The formation of bubbles induces a significant increase in the transient, capacitive, open circuit voltage through triboelectrification between the separated Ga conductive liquid metal and the DMF dielectric as previously described[12, 13]. The formation of a closed loop, by the $Ag_{0.72}Ga_{0.28}$ rods, thereafter, initiates the $CO_2$ conversion. The presence of the triboelectric effect can be validated by a proof-of-concept macro sized experiment, as depicted in Supplementary Fig. 12. The details of triboelectric voltage calculations are presented in Supplementary Information.

The $CO_2$ reduction in our system is completed through a reversible Ga-$Ga^+$ cycle. Cyclic voltammetry was conducted to provide an insight into the catalytic mechanism of the $Ag_{0.72}Ga_{0.28}$ rods *via* the suggested route. The results showed that, for the working electrode containing Ga droplets and $Ag_{0.72}Ga_{0.28}$ rods as the co-contributors, Ga is oxidized to $Ga^+$ at 0.18 V and then reduced to elemental gallium at -0.31 V (Fig. 4a)[34]. Considering that the triboelectric process generates time-dependent voltages of several volts, the carbonaceous sheets are rapidly produced on the surface of liquid metals as we have previously demonstrated[35]. We also note that $Ga^+$ reduction was not observed when either Ga droplets (Inset in Fig. 4a) or Ga droplets with non-rod morphology $Ag_{0.72}Ga_{0.28}$ were used as the working electrode (Supplementary Fig. 13), showing the importance of the long rods for the cyclic reaction.

To investigate the reaction mechanism, we performed a detailed assessment of the reaction intermediates and the by-products generated during $CO_2$ reduction. The overall reaction process in DMF is described by chemical reaction equations (1-6). The equations are separated into 'liquid metal components' reactions (equations (1-4)) and 'solid components' reactions (equations (5,6)). For the description of the liquid metal component reactions, a series of characterisations were conducted. Nuclear magnetic resonance (NMR) analysis showed that the solvent DMF was not involved in the reaction (Supplementary Fig. 14a). The $CO_2$ reduction is realised *via* the voltage provided by the nano triboelectrochemical process on the surface of Ga liquid droplets that turn Ga into $Ga^+$, while $CO_2$ is activated into the $CO_2^{\bullet-}$ radical (equation (1)). The existence of the $CO_2^{\bullet-}$ radical during the reaction is demonstrated by electron paramagnetic resonance (EPR), which uses 5,5-dimethyl-1-pyrroline N-oxide (DMPO) as a radical trapping agent to form DMPO-$CO_2^{\bullet-}$ adduct for spectroscopic analysis (Fig. 4b, see

Methods)[36]. The $CO_2$ to $CO_2^{\bullet-}$ process is followed by the generation of the intermediates CO and $O^{2-}$ radicals (equation (2))[37]. The former is further converted to carbonaceous materials on the liquid metal surface (equation (3) which is the optimum case and it can be altered according to the C to O ratio in the obtained carbonaceous solid). The equations are as follows:

$$Ga + CO_2 \rightarrow Ga^+ + CO_2^{\bullet-} \quad (1)$$

$$CO_2^{\bullet-} + Ga \rightarrow CO + Ga^+ + O^{2-} \quad (2)$$

$$CO + 2Ga \rightarrow C + 2Ga^+ + O^{2-} \quad (3)$$

$$2O^{2-} \rightarrow O_2 + 4e^- \quad (4)$$

The description of the 'solid components' reactions is as follows. According to the cyclic voltammetry results, the oxidized $Ga^+$ can be reduced to elemental Ga by receiving an electron from the $Ag_{0.72}Ga_{0.28}$ and the $Ag_{0.72}Ga_{0.28}$ turns into $Ag_{0.72}Ga_{0.28}^+$ (equation (5)). The catalytic cycle is closed by the electrons provided from the $O^{2-}$ to $O_2$ (equation (4)) to reduce $Ag_{0.72}Ga_{0.28}^+$ back to $Ag_{0.72}Ga_{0.28}$ (equation (6)), where the existence of $O_2$ can be confirmed through GC (Supplementary Fig. 4 and Supplementary Table 1).

$$4Ga^+ + 4Ag_{0.72}Ga_{0.28} \rightarrow 4Ga + 4Ag_{0.72}Ga_{0.28}^+ \quad (5)$$

$$4Ag_{0.72}Ga_{0.28}^+ + 4e^- \rightarrow 4Ag_{0.72}Ga_{0.28} \quad (6)$$

The catalytic cycle of $CO_2$ reduction at the interface of Ga droplets is illustrated in Fig. 4c. This catalytic mechanism also aligns with the DMF+ETA case, and the extra by-products are produced due to the presence of ETA that promotes the process towards CO production according to equation (5) (Supplementary Fig. 4 and Supplementary Fig. 14b)[38].

Since the reaction is activated by the triboelectric potential, other forms of mechanical stimuli can also be applied, and the system can be readily scaled up. As a demonstration, we further validate our strategy by coupling an overhead stirrer to a 50 mL reactor. We found that $CO_2$ conversion continuously takes place in a stable manner when the stirring speed exceeds a threshold of 200 rpm (at room temperature, Supplementary Fig. 15a) and the conversion efficiency increases along with the increase of the stirring speed (equivalently, the mechanical energy input) (Supplementary Table 1 and Supplementary Fig. 15b,c).

# Conclusion

In conclusion, we demonstrated a promising mechanical energy-induced $CO_2$ conversion method which operates solely with mechanical stimuli. The catalytic process was found to be mechanically enabled by co-contributors containing liquid metal Ga droplets and resilient intermetallic $Ag_{0.72}Ga_{0.28}$ structures. We demonstrated the crucial roles of the composition and morphology of the functional materials, as well as the importance of precursor selection for triboelectrochemical $CO_2$ conversion. The obtained $CO_2$ capture and conversion efficiency was 92% for a reactor with a height as small as 27 cm at the input $CO_2$ flow rate of ~8 sccm.

The prospects of further exploring the proposed system are extensive. This methodology can be extended for large-scale systems and long-term operation by employing different forms of mechanical energies. This methodology with its remarkable capabilities provides promising prospects for future practical deployment of $CO_2$ conversion technologies. Altogether, the novel concept provided by this new system offers a platform to fundamentally impact the future of carbon capture technologies and relevant industries.

# Declarations


### Acknowledgments

This work was supported by the Australian Research Council (ARC) Laureate Fellowship grant (FL180100053), the ARC Center of Excellence FLEET (CE170100039) and Chevron. The authors would like to thank Dr. Yin Yao, Dr. Sean Lim of the Electron Microscope Unit within the Mark Wainwright Analytical Centre at UNSW Sydney, and Dr. Donald Thomas of the Spectroscopy Laboratory and the Nuclear Magnetic Resonance Facility for their technical assistance.


### Author contributions

J.T., D.E., and K.K.-Z. initiated the concept and designed the experiments. J.T. conducted the experiments and carried out the characterisations with the help of J.T., M.M., M.B., J.S., M.A.R., J.H., D.J.L, and R.J. The following individuals contributed to the data analyses, scientific discussions and authorship of the paper: J.T., J.T., T.D., A.P.O., R.B.K., D.E., M.D.D., K.K.-Z. All authors revised the manuscript and provided helpful comments.

### Competing interests

The authors declare no competing interests.

### Additional information


Correspondence and requests for materials should be addressed to K.K.-Z.


# References

1. Mukherjee, S. *et al.* Trace $CO_2$ capture by an ultramicroporous physisorbent with low water affinity. *Sci. Adv.* **5,** eaax9171 (2019).
2. García de Arquer, F. P. *et al.* $CO_2$ electrolysis to multicarbon products at activities greater than 1 A $cm^{-2}$. *Science* **367,** 661-666 (2020).
3. Gao, S. *et al.* Partially oxidized atomic cobalt layers for carbon dioxide electroreduction to liquid fuel. *Nature* **529,** 68 (2016).
4. Li, C. W., Ciston, J., Kanan, M. W. Electroreduction of carbon monoxide to liquid fuel on oxide-derived nanocrystalline copper. *Nature* **508,** 504-507 (2014).
5. Li, X. *et al.* Selective visible-light-driven photocatalytic $CO_2$ reduction to $CH_4$ mediated by atomically thin $CuIn_5S_8$ layers. *Nat. Energy* **4,** 690-699 (2019).
6. Wu, Y., Jiang, Z., Lu, X., Liang, Y., Wang, H. Domino electroreduction of $CO_2$ to methanol on a molecular catalyst. *Nature* **575,** 639-642 (2019).
7. Nahar, S., Zain, M. F. M., Kadhum, A. A. H., Hasan, H. A., Hasan, M. R. Advances in Photocatalytic $CO_2$ Reduction with Water: A Review. *Materials (Basel)* **10,** (2017).
8. Liu, X. *et al.* Understanding trends in electrochemical carbon dioxide reduction rates. *Nat. Commun.* **8,** 15438 (2017).
9. Stuart, M. A. *et al.* Emerging applications of stimuli-responsive polymer materials. *Nat. Mater.* **9,** 101-113 (2010).
10. Gan, T. *et al.* Liquid Metal-Mediated Mechanochemical Polymerization. *Macromol Rapid Commun.* **40,** e1900537 (2019).
11. You, S., Chen, M. W., Dlott, D. D., Suslick, K. S. Ultrasonic hammer produces hot spots in solids. *Nat. Commun.* **6,** 6581 (2015).
12. Zou, H. *et al.* Quantifying the triboelectric series. *Nat. Commun.* **10,** 1427 (2019).
13. Yang, Y. *et al.* Single-Electrode-Based Sliding Triboelectric Nanogenerator for Self-Powered Displacement Vector Sensor System. *ACS Nano* **7,** 7342-7351 (2013).
14. Wang, Z. L. On Maxwell's displacement current for energy and sensors: the origin of nanogenerators. *Mater. Today* **20,** 74-82 (2017).
15. Asadi, M. *et al.* Robust carbon dioxide reduction on molybdenum disulphide edges. *Nat. Commun.* **5,** 4470 (2014).
16. Li, H. *et al.* Colloidal silver diphosphide ($AgP_2$) nanocrystals as low overpotential catalysts for $CO_2$ reduction to tunable syngas. *Nat. Commun.* **10,** 5724 (2019).
17. Morales-Guio, C. G. *et al.* Improved $CO_2$ reduction activity towards $C_{2+}$ alcohols on a tandem gold on copper electrocatalyst. *Nat. Catal.* **1,** 764-771 (2018).
18. Esrafilzadeh, D. *et al.* Room temperature $CO_2$ reduction to solid carbon species on liquid metals featuring atomically thin ceria interfaces. *Nat. Commun.* **10,** 865 (2019).

19. Torelli, D. A. *et al.* Nickel–Gallium-Catalyzed Electrochemical Reduction of $CO_2$ to Highly Reduced Products at Low Overpotentials. *ACS Catal.* **6,** 2100-2104 (2016).
20. Losurdo, M., Suvorova, A., Rubanov, S., Hingerl, K., Brown, A. S. Thermally stable coexistence of liquid and solid phases in gallium nanoparticles. *Nat. Mater.* **15,** 995-1002 (2016).
21. Markvicka, E. J., Bartlett, M. D., Huang, X., Majidi, C. An autonomously electrically self-healing liquid metal–elastomer composite for robust soft-matter robotics and electronics. *Nat. Mater.* **17,** 618-624 (2018).
22. Qin, B., Schneider, U. Catalytic Use of Elemental Gallium for Carbon-Carbon Bond Formation. *J. Am. Chem. Soc.* **138,** 13119-13122 (2016).
23. Jitaru, M. Electrochemical carbon dioxide reduction - Fundamental and applied topics. *J. Univ. Chem. Technol. Metallurgy* **42,** 333-344 (2007).
24. Daeneke, T. *et al.* Liquid metals: fundamentals and applications in chemistry. *Chem. Soc. Rev.* **47,** 4073-4111 (2018).
25. Park, J.-Y., Yoon, S. J., Lee, H. Effect of Steric Hindrance on Carbon Dioxide Absorption into New Amine Solutions: Thermodynamic and Spectroscopic Verification through Solubility and NMR Analysis. *Environ. Sci. Technol.* **37,** 1670-1675 (2003).
26. Chen, L. *et al.* Modifying graphite oxide nanostructures in various media by high-energy irradiation. *RSC Adv.* **4,** 1025-1031 (2014).
27. House, K. Z. *et al.* Economic and energetic analysis of capturing $CO_2$ from ambient air. *Proc. Natl. Acad. Sci. U. S. A.* **108,** 20428 (2011).
28. Kätelhön, A., Meys, R., Deutz, S., Suh, S., Bardow, A. Climate change mitigation potential of carbon capture and utilization in the chemical industry. *Natl. Acad. Sci. U. S. A.* **116,** 11187 (2019).
29. Keith, D. W., Holmes, G., St. Angelo, D., Heidel, K. A Process for Capturing $CO_2$ from the Atmosphere. *Joule* **2,** 1573-1594 (2018).
30. Sen, R., Goeppert, A., Kar, S., Prakash, G. K. S. Hydroxide Based Integrated $CO_2$ Capture from Air and Conversion to Methanol. *J. Am. Chem. Soc.* **142,** 4544-4549 (2020).
31. Ye, R.-P. *et al.* $CO_2$ hydrogenation to high-value products via heterogeneous catalysis. *Nat. Commun.* **10,** 5698 (2019).
32. Zhang, J. *et al.* Effect of Support on the Activity of Ag-based Catalysts for Formaldehyde Oxidation. *Sci. Rep.* **5,** 12950 (2015).
33. Li, Y., Bettge, M., Bareño, J., Trask, S. E., Abraham, D. P. Exploring Electrochemistry and Interface Characteristics of Lithium-Ion Cells with $Li_{1.2}Ni_{0.15}Mn_{0.55}Co_{0.1}O_2$Positive and $Li_4Ti_5O_{12}$Negative Electrodes. *J. Electrochem. Soc.* **162,** A7049-A7059 (2015).
34. Bard, A. J., Parsons, R., Jordan, J. *Standard Potentials in Aqueous Solutions*. IUPAC: New York, USA, 1985.
35. Mayyas, M. *et al.* Liquid-Metal-Templated Synthesis of 2D Graphitic Materials at Room Temperature. *Adv. Mater.* 2001997 (2020).

36. Villamena, F. A., Locigno, E. J., Rockenbauer, A., Hadad, C. M., Zweier, J. L. Theoretical and Experimental Studies of the Spin Trapping of Inorganic Radicals by 5,5-Dimethyl-1-Pyrroline N-Oxide (DMPO). 1. Carbon Dioxide Radical Anion. *J. Phys. Chem. A* **110,** 13253-13258 (2006).
37. Ijije, H. V., Lawrence, R. C., Chen, G. Z. Carbon electrodeposition in molten salts: electrode reactions and applications. *RSC Adv.* **4,** 35808-35817 (2014).
38. Zhang, S. *et al.* Polyethylenimine-enhanced electrocatalytic reduction of $CO_2$ to formate at nitrogen-doped carbon nanomaterials. *J. Am. Chem. Soc.* **136,** 7845-7848 (2014).

# Methods

**Materials.** Gallium (Ga, ingot, purity: 99.99%) was purchased from Rotometals, USA, and silver powder (purity: 99.9%) was obtained from Sigma-Aldrich. All the salts, including AgF, AgCl, AgBr, AgI, AgOTf, $AgNO_3$, KCl, NaCl and $NaHCO_2$, were obtained from Sigma-Aldrich with a purity of 99.5%. The solvents DMF (purity: 99.8%, boiling point: 153 °C), ETA (purity: ~ 98%, boiling point: 170 °C) and HCl (33 wt% in water) were acquired from Chem-Supply Pty Ltd. $HNO_3$ (acidimetric: ≥ 65.0%), DMPO (purity: 99.9%) and $H_2O_2$ (30 wt% in water) were purchased from Sigma-Aldrich. Milli-Q water was used throughout the experiments for sample preparation and reaction.

**Preparation of functional materials.** (1) Sliver salts as precursors: During a typical co-contributor preparation process (using AgF as an example), Ga (7.0 g) was first added into a glass vial which is pre-filled with 5.0 mL DMF solution, followed by adding HCl solution to give a final 0.10 M to remove the surface oxide layer of Ga. AgF (1.0 g) was then added to the mixture as the precursor.

(2) Ag (150 nm particle size) as precursors: For the preparation of Ag-Ga alloy, the silver powder was added to Ga (7.0 g) in concentrations of 2.0 wt% and 5.0 wt%, respectively. The mixtures were ground using a mortar and pestle inside a $N_2$-filled glove box to minimize oxidation of the liquid metal[18]. The grinding process, typically lasts 40 min, was stop until the sample showed a smooth and reflective appearance.

(3) Probe sonication procedures: The mixture from step (1) or step (2) was sonicated with a probe sonicator (VC 750, Sonics & Materials) under the protection of $N_2$. The sonication amplitude was set to 55%, corresponding to an ultrasonic power input of ~410 W. The sonicator was paused for 1 s after each 9 s sonication and the total sonication time was 30 min.

**$CO_2$ conversion experiment.** (1) Bath sonication as the energy source: After the preparation of functional material, $CO_2$ was bubbled into the reactor through a diffuser and the flow rate of $CO_2$ gas (10 sccm) was controlled using a gas mass flow controller (MKS, GE50A). Bath sonication (FREQ 50Hz, Unisonics) was employed as the mechanical energy source to trigger $CO_2$ conversion. The temperature of the reaction solution was kept around 40 °C during the 5 hours reaction.

(2) Overhead stirrer as the energy source: When $CO_2$ was bubbled into the reactor through a diffuser at the same rate of 10 sccm, an overhead stirrer (DLS Digital Overhead Stirrer, 120 W) was utilized as the mechanical energy source. Different rotation speeds, including 200, 300, 400, 500 and 1000 rpm, were applied for initiating the $CO_2$ conversion. The experiment was performed at room temperature for 24 hours.

**Sample characterisations.** Raman spectra were collected via a Raman spectrometer (Via Raman microscope, Renishaw) utilizing the 532 nm laser source. XPS was performed on a Thermo Scientific K-alpha X-ray spectrometer. The carbon product was studied using micro-FTIR spectroscopy, on a PerkinElmer Spectrum 100 FTIR Spectrometer which is coupled to a Spotlight 400 FTIR Imaging System with stage controller. The morphology and structure of materials were imaged by SEM (JEOL JSM-IT-500 HR). The TEM and SAED characterisations were performed on a Phillips CM200 TEM system. Both the SEM and the TEM systems are coupled with an EDS detector for elemental and compositional analysis. The crystalline phases of the samples were characterised by XRD (Philips X'Pert Pro MPD, λ = 1.54 Å, Cu-Kα radiation). The TGA for carbonaceous material quantification was performed on a Thermogravimetric Analyzer TGA Q5000 IR. ICP-MS was performed on NexION 2000 B ICP Mass Spectrometer to determine the concentration of gallium and silver ions. EPR experiments for the detection of the $CO_2^{\bullet-}$ radicals were conducted on a Bruker EMX X-Band ESR Spectrometer (Bohr). NMR experiments were performed to investigate the liquid species in the solution, which was performed by using Bruker Avance III 600 MHz Cryo NMR (Ernst).

**Preparation and analysis of TGA samples.** The carbonaceous materials for the TGA experiments were separated by centrifugation. After a specific reaction time ($T$, h), the homogeneous mixture from the reactor (2.0 mL) was added into a centrifuge tube followed by centrifuging at a speed of 10000 rpm for 10 min. During this process, the suspended solid materials were separated into different layers. Most of the metallic catalysts deposit at the bottom of the tube due to their high density, in comparison to the carbonaceous materials which remains suspended in the top layer. The centrifugation process was repeated three times and each time the carbon-containing top layer was collected. The collected materials (sample volume $V_{TGA}$ = 2.0 mL solution during certain reaction time $T$ (h)) were then dried (110 °C) to remove DMF from the samples before the TGA experiments. During the TGA experiments, the heating rate was set to 10 °C/min and the upper temperature limit was fixed at 800 °C.

**ICP-MS samples:** During the process of $CO_2$ reduction, 1.0 mL reaction mixture was taken as a sample every hour and then we centrifuged the sample for 15 min at 10000 rpm until all the suspended materials deposit at the bottom of the tube. Then, we took 0.20 mL clear solution from the top of the sample and heated it on the hot plate until it was completely dried. Thereafter, 0.20 mL of nitric acid was added to dissolve the residue for ICP-MS.

**Cyclic voltammetry experiments:** Cyclic voltammetry experiments were conducted to investigate the roles of the $Ag_{0.72}Ga_{0.28}$ rods during the $CO_2$ reduction. Ga droplets and $Ag_{0.72}Ga_{0.28}$ rods were obtained from the Ga and AgF precursors. Then, we painted the Ga/$Ag_{0.72}Ga_{0.28}$ ($Ag_{0.72}Ga_{0.28}$ in the shape of a rod) on

fluorine doped tin oxide (FTO) and baked it until the material dried and immobilised on the FTO as the working electrode. A calomel reference electrode and a gold counter electrode were used to set up a three-electrode configuration. DMF+ETA solution containing 0.10 M HCl was utilized as the electrolyte to keep the condition consistent to the reaction situation. As a comparison, Ga droplets and Ga/$Ag_{0.72}Ga_{0.28}$ ($Ag_{0.72}Ga_{0.28}$ with non-rod morphology, using Ga/AgI) were painted on FTO as the working electrode respectively and all other parameters were kept identical.

**EPR experiments:** To provide mechanistic insights, EPR experiments were conducted to confirm the existence of the activated $CO_2$. DMPO is known as a standard $CO_2^{\bullet-}$ radical captor and the combination of DMPO with the $CO_2^{\bullet-}$ radical shows characteristic signals[36,39]. During the experiments, 20 mg DMPO was added and dissolved into 5.0 mL Milli-Q water and then 1.0 mL DMPO solution was further added into the reaction system. After bubbling $CO_2$ into the solution in the presence of bath sonication for 30 min, 1.0 mL reaction solution was centrifuged to remove all the suspended materials for EPR measurement. As a control, 1.0 mL DMPO solution was added into the reaction system in the process of bath sonication without bubbling $CO_2$.

To verify that the EPR signal obtained from our reaction system was due to the formation of $CO_2^{\bullet-}$, an independent reaction involving $CO_2^{\bullet-}$ formation is further conducted. It is well established that the $CO_2^{\bullet-}$ radical can be generated from $NaHCO_2$ and $H_2O_2$ under the irradiation of ultraviolet light[36]. $NaHCO_2$ and 30% $H_2O_2$ were dissolved in 5.0 mL Milli-Q water in the concentration of 100 mM and 100 μM, respectively, with the DMPO concentration being 50 mM. After irradiation with ultraviolet light for 10 min, we mixed 1.0 mL photolytic solution with 20 mL DMF solution for EPR analysis to keep the condition consistent with the conditions of our $CO_2$ conversion reaction. By comparison, the EPR spectra from the reaction system and photolytic solution were in good agreement, thereby validating the existence of $CO_2^{\bullet-}$ radical during our $CO_2$ conversion reaction (Fig. 4c).

## Data availability

The datasets generated during the current study are available from the corresponding authors upon reasonable request.

## References

39. Barbieriková, Z., Dvoranová, D., Brezová, V. Photoinduced transformation of glycerol in titania suspensions. (An EPR spin trapping study of radical intermediates). *Catal. Today* **313,** 106-113 (2018).

# Figures

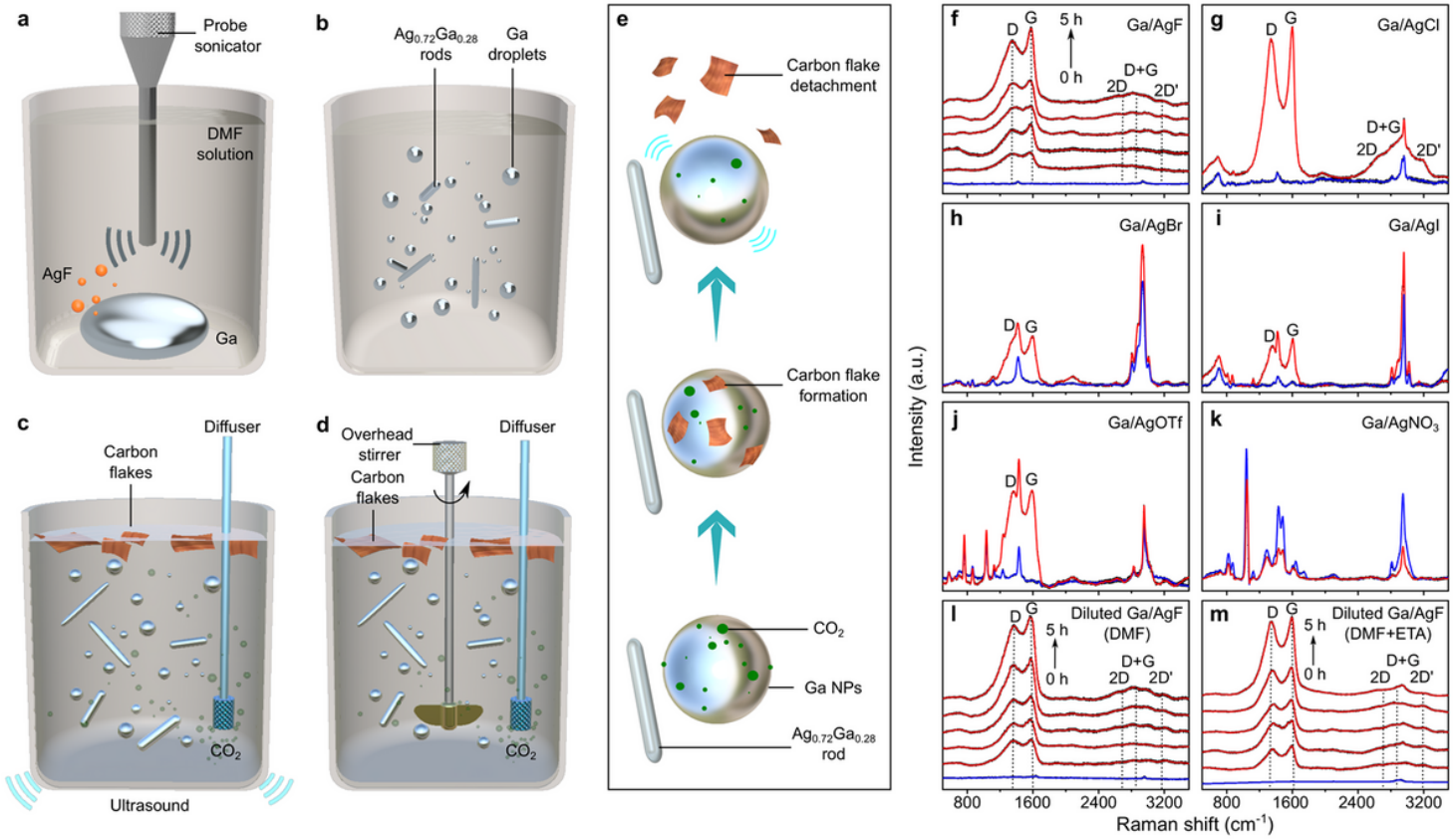


## Figure 1

Schematics and Raman spectra of solid carbon produced from CO2 using liquid metal. a-d, Schematic illustrations for the preparation of a suspension of catalyst (a,b) and the CO2 reduction process using different mechanical energy inputs (c,d). e, Schematic illustration of the formation and detachment of carbon flakes on the surface of Ga droplets in the presence of the solid rods. f-k, Raman spectra of the samples obtained from the reaction mixes of Ga with different silver salts as precursors in DMF: AgF (f, versus time), AgCl (g), AgBr (h), AgI (i), AgOTf (j) and AgNO3 (k). The D and G bands at 1350 and 1600 cm-1, respectively, emerged after the reactions occur. l,m, Raman spectra (versus time) from the surface of mixtures from the 10-times diluted reaction system (Ga and AgF mix) by employing DMF (l) and DMF+ETA (m) as the reaction solutions. The blue and red curves in f-m are Raman spectra for the samples before and after reaction, respectively.

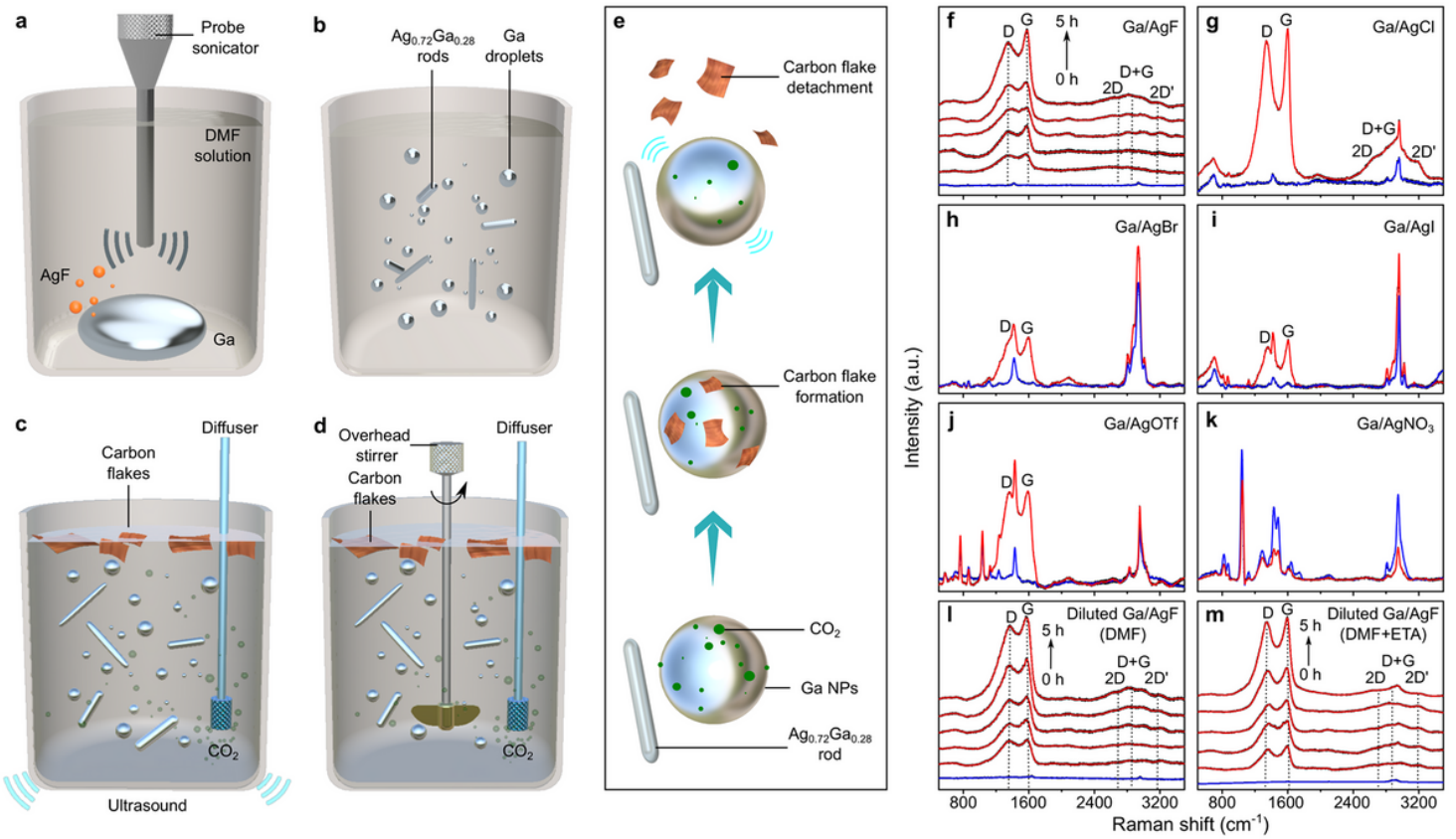


## Figure 1

Schematics and Raman spectra of solid carbon produced from CO2 using liquid metal. a-d, Schematic illustrations for the preparation of a suspension of catalyst (a,b) and the CO2 reduction process using different mechanical energy inputs (c,d). e, Schematic illustration of the formation and detachment of carbon flakes on the surface of Ga droplets in the presence of the solid rods. f-k, Raman spectra of the samples obtained from the reaction mixes of Ga with different silver salts as precursors in DMF: AgF (f, versus time), AgCl (g), AgBr (h), AgI (i), AgOTf (j) and AgNO3 (k). The D and G bands at 1350 and 1600 cm-1, respectively, emerged after the reactions occur. l,m, Raman spectra (versus time) from the surface of mixtures from the 10-times diluted reaction system (Ga and AgF mix) by employing DMF (l) and DMF+ETA (m) as the reaction solutions. The blue and red curves in f-m are Raman spectra for the samples before and after reaction, respectively.

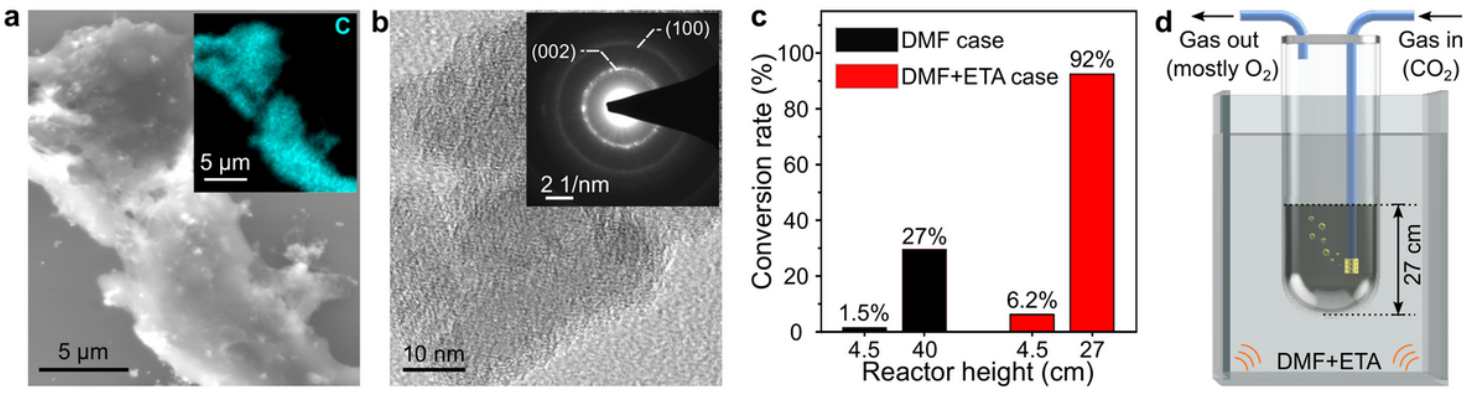

## Figure 2

Characterisations of the carbonaceous products (a-b) and the demonstration of the scalability of the technology (c-e). a, SEM and EDS images (inserted in a) of the carbonaceous materials. b, TEM and SAED (inserted in b) images of the separated carbonaceous products. c, Conversion efficiencies of CO2 under different configurations showing the maximum efficiency of 92% for CO2 capture and conversion in DMF+ETA case. d, Schematic representations of the scaled-up reactors for full CO2 conversion for DMF+ETA reactors (refer to Supplementary Information for the actual picture of the 27 cm reactor).

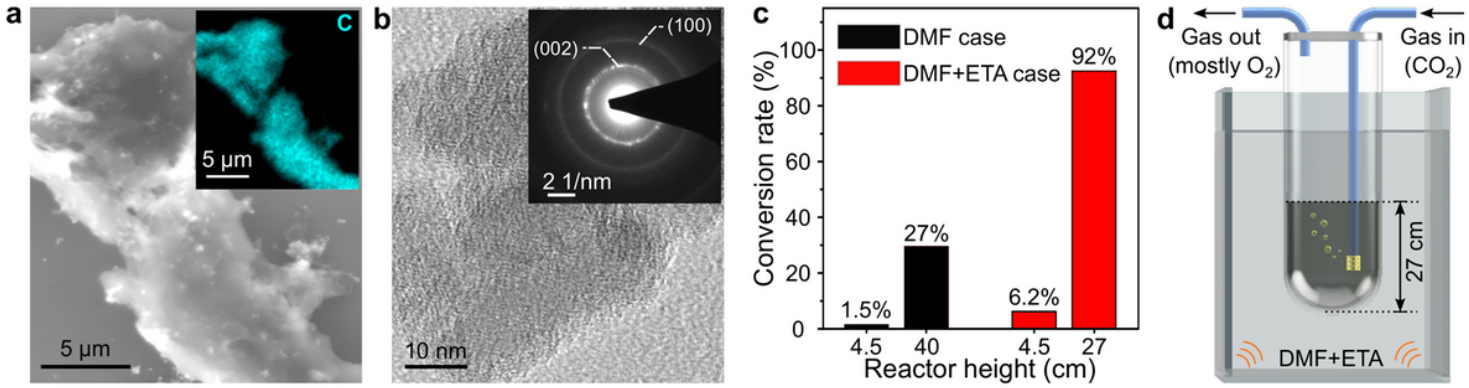


## Figure 2

Characterisations of the carbonaceous products (a-b) and the demonstration of the scalability of the technology (c-e). a, SEM and EDS images (inserted in a) of the carbonaceous materials. b, TEM and SAED (inserted in b) images of the separated carbonaceous products. c, Conversion efficiencies of CO2 under different configurations showing the maximum efficiency of 92% for CO2 capture and conversion in DMF+ETA case. d, Schematic representations of the scaled-up reactors for full CO2 conversion for DMF+ETA reactors (refer to Supplementary Information for the actual picture of the 27 cm reactor).

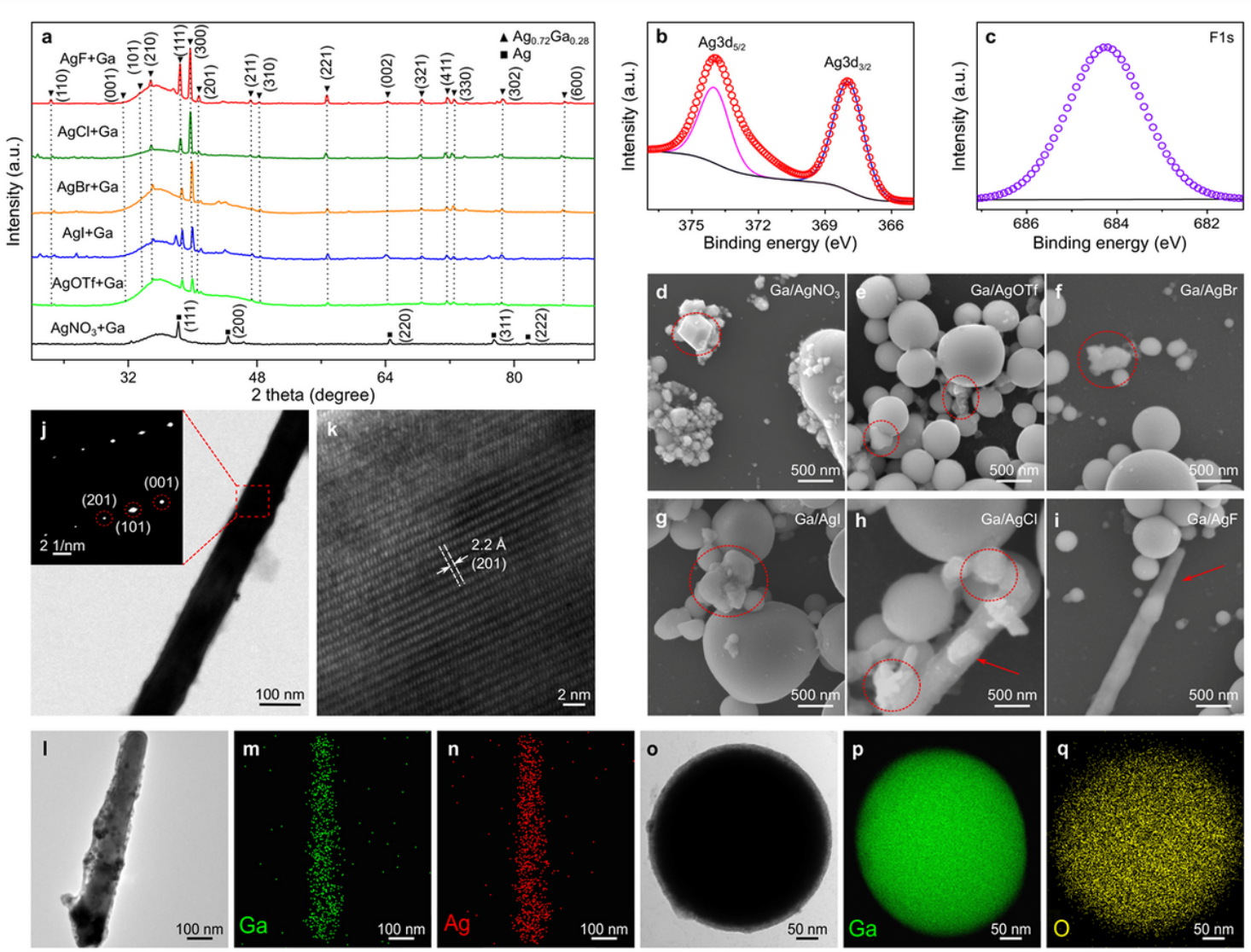


## Figure 3

Characterisation of the functional materials. a, XRD patterns after probe sonication by employing different silver salts with Ga as the precursors. Except for Ga/AgNO3, the other silver salts and Ga were converted into Ag0.72Ga0.28. b,c, XPS analysis of the state of silver and fluoride on the surface of the mixtures after probe sonication. d-i, SEM images of the materials after probe sonication when different silver salts were used as precursors as Ga/AgNO3 (d), Ga/AgOTf (e), Ga/AgBr (f), Ga/AgI (g), Ga/AgCl (h), and Ga/AgF (i). Ag0.72Ga0.28 was found in the shape of rods only when AgF was used as the precursor, and some rods were also seen for the AgCl case, while Ag0.72Ga0.28 from other silver salts have non-rod morphologies. j,k, TEM and HRTEM of Ag0.72Ga0.28 nanorods with SAED images inserted in j. l-q, TEM and corresponding EDS images of Ag0.72Ga0.28 rods and Ga droplets.

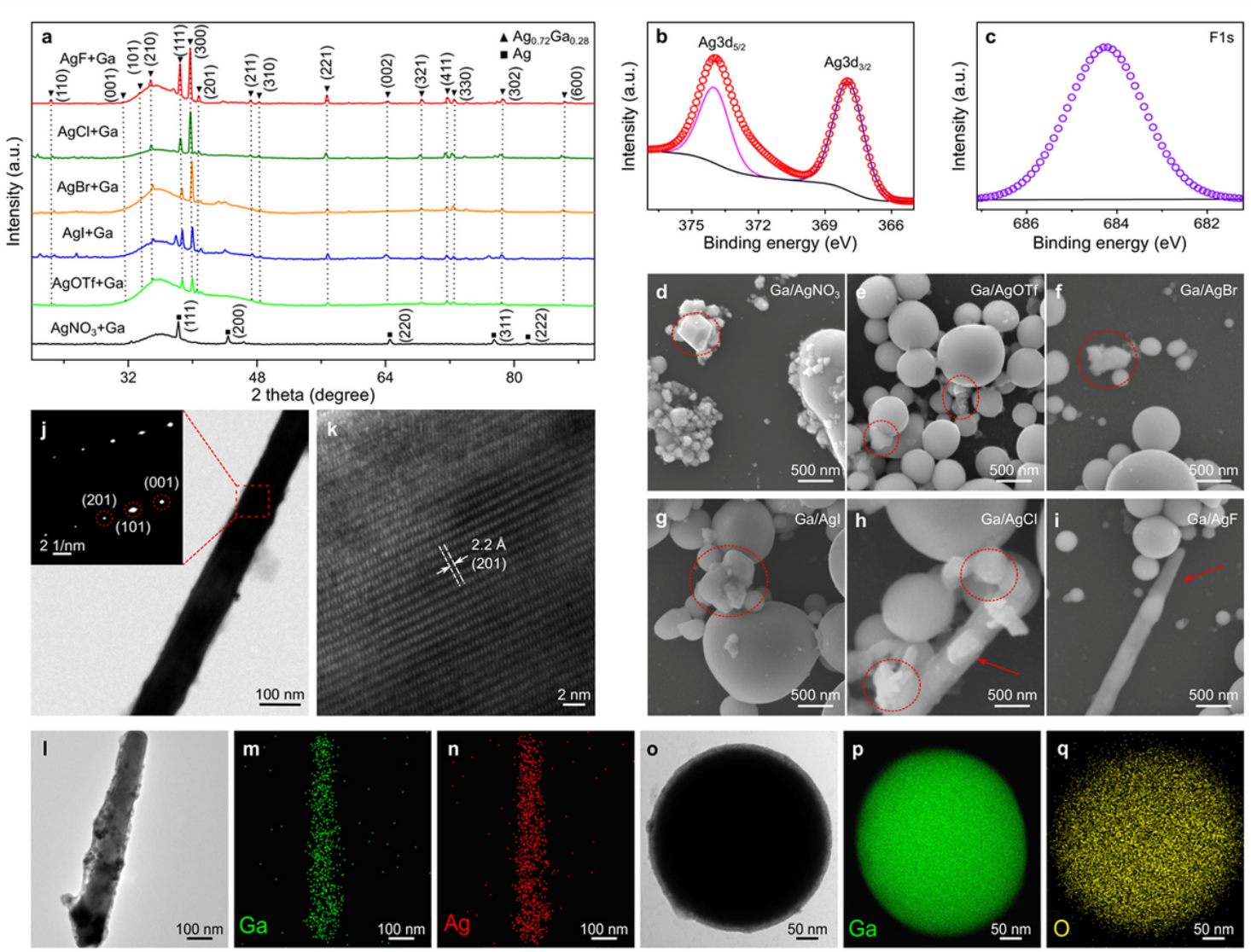


## Figure 3

Characterisation of the functional materials. a, XRD patterns after probe sonication by employing different silver salts with Ga as the precursors. Except for Ga/AgNO3, the other silver salts and Ga were converted into Ag0.72Ga0.28. b,c, XPS analysis of the state of silver and fluoride on the surface of the mixtures after probe sonication. d-i, SEM images of the materials after probe sonication when different silver salts were used as precursors as Ga/AgNO3 (d), Ga/AgOTf (e), Ga/AgBr (f), Ga/AgI (g), Ga/AgCl (h), and Ga/AgF (i). Ag0.72Ga0.28 was found in the shape of rods only when AgF was used as the precursor, and some rods were also seen for the AgCl case, while Ag0.72Ga0.28 from other silver salts have non-rod morphologies. j,k, TEM and HRTEM of Ag0.72Ga0.28 nanorods with SAED images inserted in j. l-q, TEM and corresponding EDS images of Ag0.72Ga0.28 rods and Ga droplets.

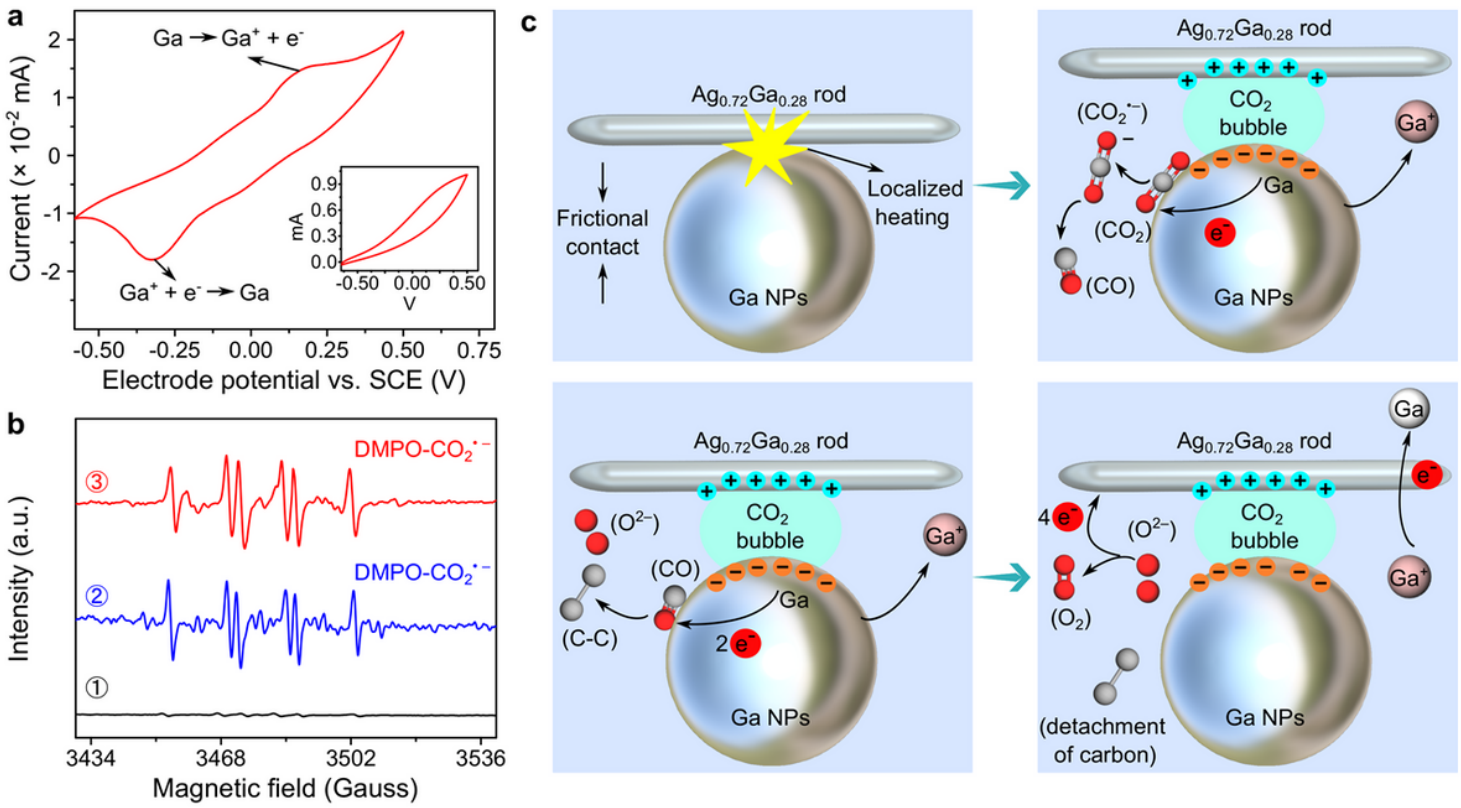


## Figure 4

Reaction mechanism of CO2 reduction. a, Cyclic voltammetry curve of the Ga+-Ga cycle with Ga droplets and Ag0.72Ga0.28 rods as the working electrode. Inset: Cyclic voltammetry curve with only Ga droplets as the working electrode. b, EPR spectra of the carbon dioxide radical (CO2•−) addition to DMPO. ( Spectrum of DMPO added into the reaction solution for 30 min without bubbling CO2.  Spectrum of DMPO-CO2•− by ultraviolet photolysis of 100 mM NaHCO2 and 100 μM H2O2 in the presence of 50 mM DMPO in Milli-Q water for 10 min, followed by the addition of photolytic 1.0 mL solution into 20 mL DMF for EPR analysis.  Spectrum of DMPO-CO2•− with DMPO added into the reaction solution for 30 min when CO2 reduction is proceeding). c, Proposed catalytic cycle for CO2 reduction on the surface of Ga droplets with Ag0.72Ga0.28 rods working as the functional material.

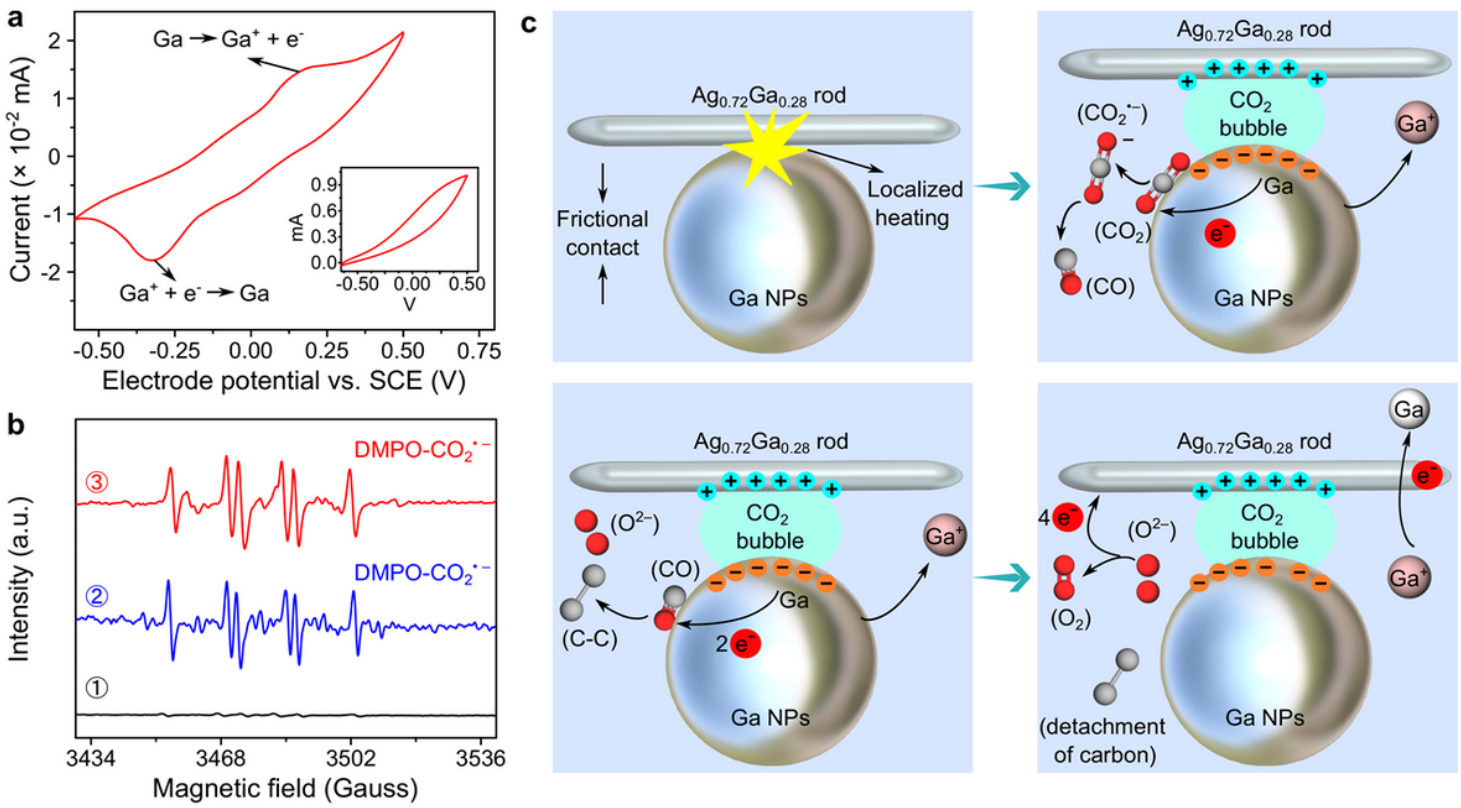


**Figure 4**

Reaction mechanism of CO2 reduction. a, Cyclic voltammetry curve of the Ga+-Ga cycle with Ga droplets and Ag0.72Ga0.28 rods as the working electrode. Inset: Cyclic voltammetry curve with only Ga droplets as the working electrode. b, EPR spectra of the carbon dioxide radical (CO2•−) addition to DMPO. ( Spectrum of DMPO added into the reaction solution for 30 min without bubbling CO2.  Spectrum of DMPO-CO2•− by ultraviolet photolysis of 100 mM NaHCO2 and 100 μM H2O2 in the presence of 50 mM DMPO in Milli-Q water for 10 min, followed by the addition of photolytic 1.0 mL solution into 20 mL DMF for EPR analysis.  Spectrum of DMPO-CO2•− with DMPO added into the reaction solution for 30 min when CO2 reduction is proceeding). c, Proposed catalytic cycle for CO2 reduction on the surface of Ga droplets with Ag0.72Ga0.28 rods working as the functional material.

# Supplementary Files

This is a list of supplementary files associated with this preprint. Click to download.

- NatureCatalysisSupplementary.docx
- NatureCatalysisSupplementary.docx